



Contents lists available at ScienceDirect
Spectrochimica Acta Part A:
Molecular and Biomolecular Spectroscopy

journal homepage: www.journals.elsevier.com/spectrochimica-acta-part-a-molecular-and-biomolecular-spectroscopy



High resolution spectroscopy of $B\ 0_u^+ \leftarrow X\ 0_g^+$ transitions in $^{130}\text{Te}_2$: Reference lines spanning the 443.2–451.4 nm region

Qinning Lin ^{a,1}, Jie Ma ^{a,1}, James Coker ^b, Renjun Pang ^a, Zesen Wang ^a, J.E. Furneaux ^{b,*}, Jianping Yin ^a, Tao Yang ^{a,c,d,*}

^a State Key Laboratory of Precision Spectroscopy, East China Normal University, Shanghai 200062, PR China

^b Homer L. Dodge Department of Physics and Astronomy, University of Oklahoma, Norman, OK 73019, USA

^c Xinjiang Astronomical Observatory, Chinese Academy of Sciences, 150 Science 1 – Street, Urumqi, Xinjiang 830011, PR China

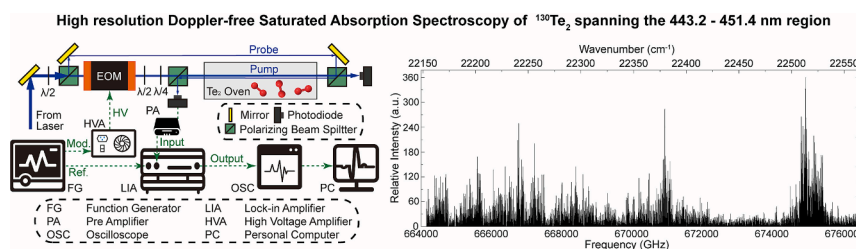
^d Collaborative Innovation Center of Extreme Optics, Shanxi University, Taiyuan, Shanxi 030006, PR China



HIGHLIGHTS

- We measured 9294 transition lines of $^{130}\text{Te}_2$ via the Doppler-free Saturated Absorption Spectroscopy spanning the 443.2–451.4 nm region.
- We assigned 1899 transition lines using the Dunham model, and reported diatomic constants for the $B\ (^3\Sigma_u^-)\ 0_u^+$ state.
- A high resolution spectral atlas of $^{130}\text{Te}_2$ can have applications as a frequency reference.

GRAPHICAL ABSTRACT



ARTICLE INFO

Keywords:

Diatomeric molecules
 Tellurium spectrum
 Saturated absorption spectroscopy
 Frequency reference

ABSTRACT

Molecular tellurium ($^{130}\text{Te}_2$) has long been regarded as a promising candidate for a variety of spectroscopic applications, especially as a frequency reference. Absorption lines of $^{130}\text{Te}_2$ were published extensively in the past few decades, however, the spectral resolution was not sufficiently high to be considered a precision spectroscopic reference. Here, a high resolution spectral atlas of $^{130}\text{Te}_2$ Doppler-free saturated absorption transitions is reported, and used to assign multiple ro-vibrational bands in the $B\ (^3\Sigma_u^-)\ 0_u^+ \leftarrow X\ (^3\Sigma_u^-)\ 0_g^+$ electronic transition via the Dunham model, giving updated Dunham parameters and diatomic constants for the $B\ (^3\Sigma_u^-)\ 0_u^+$ state at an unprecedented level of precision. Our findings reveal spectroscopic properties of $^{130}\text{Te}_2$ that might eventually contribute to frequency reference in precision measurement such as the quest for non-zero electron's Electric Dipole Moment (eEDM).

1. Introduction

Molecular tellurium (Te_2) offers a broad range of potential

applications. As a paramagnetic molecule, molecular tellurium has been utilized to study quadratic corrections to the Zeeman effect, alignment-orientation conversion, and cooperative processes such as super-

* Corresponding authors at: State Key Laboratory of Precision Spectroscopy, East China Normal University, Shanghai 200062, PR China (T. Yang) and Homer L. Dodge Department of Physics and Astronomy, University of Oklahoma, Norman, OK 73072, USA (J.E. Furneaux).

E-mail addresses: furneaux@ou.edu (J.E. Furneaux), tyang@lps.ecnu.edu.cn (T. Yang).

¹ Qinning Lin and Jie Ma contributed to the work equally.

<https://doi.org/10.1016/j.saa.2024.123887>

Received 16 July 2023; Received in revised form 21 November 2023; Accepted 10 January 2024

Available online 14 January 2024

1386-1425/© 2024 Elsevier B.V. All rights reserved.

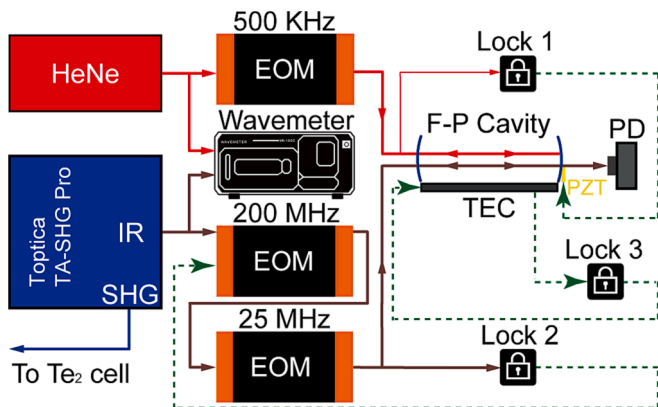


Fig. 1. Experimental setup for the frequency stabilization system (Not to scale). Red: HeNe laser beam; Brown: fundamental infrared (IR) laser beam (~ 890 nm); Blue: Second Harmonic Generation (SHG) laser beam (~ 445 nm); Green dashed: electrical signal. (For interpretation of the references to color in this figure legend, the reader is referred to the web version of this article.)

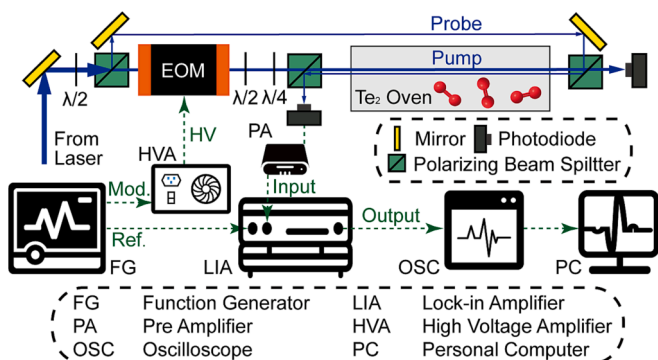


Fig. 2. Experimental setup for the Doppler-free SAS measurement surrounding the tellurium cell (not to scale). Blue: SHG output (~ 445 nm); green dashed: electrical signal. (For interpretation of the references to color in this figure legend, the reader is referred to the web version of this article.)

fluorescence [1,2]. At the same time, spectroscopic investigations of its excited states ($A\ 1_u$ and $B\ 0_u^+$) including lifetimes, cross-sections and Lande factors were conducted via a global deperturbation analysis [3,4]

and the Hanle-effect [5,6]. Also, dissociation results from mass spectrometric studies of Te_2 vapor are in excellent agreement with photoionization and spectroscopic methods [7].

Atomic and molecular absorption lines are conveniently used as the effective absolute frequency standards in modern optics [8]. Molecular tellurium absorption lines cover the range between 350 and 600 nm [9,10]. A comprehensive absorption database was collected by J. Cariou and P. Luc [11]. In 1972, Barrow *et al.* observed absorption and fluorescence spectra of Te_2 , and then made a detailed rotational analysis of 114 absorption bands as well as their associated diatomic constants [12,13]. Ten years later, Vergès *et al.* recorded the laser induced fluorescence spectra of Te_2 with Fourier transform spectrometry and analyzed the transitions involving four upper states ($A\ 0_u^+$, $B\ 0_u^+$ and 1_u components of two other states) and three lower states ($X\ 0_g^+$, $X\ 1_g$ and $b\ 1\Sigma_g^+$), as well as their associated molecular constants using simultaneous least squares fitting [14,15]. Stolyarov *et al.* studied the effects of perturbations on the term values and the rotational intensity distribution [4] while Martinez *et al.* measured the fluorescence lifetimes of the excited states ($A\ 1_u$ and $B\ 0_u^+$) of Te_2 in 1990 [16]. More recent studies of Te_2 provide a few reference lines for frequency stabilization. These studies include Saturated Absorption Spectroscopy (SAS) or Modulation Transfer Spectroscopy (MTS) techniques, providing Te_2 frequency standards in the 400–600 nm range for multiple purposes, including but not limited to the measurement of electron's Electric Dipole Moment (*e*EDM) using PbF molecules [17,18], the design of a nearly drift-free barium-ion trap [19,20], a study of the fluorescence spectrum of indium [21] and calcium [22], elementary particle studies involving muonium [23] and positronium [24], a high-accuracy wavelength reference for both Stilbene 420 dye-tuning [25] and Ar^+ laser stabilization [26], precision spectroscopy of single trapped Yb^+ ions [27] and frequency standards for both Balmer- β transitions and two-photon transitions in hydrogen and deuterium [28]. However, these studies only reported a few high-resolution transition lines [29].

Therefore, we present an updated, high-resolution catalogue of $^{130}Te_2$ Doppler-free SAS transitions, and demonstrate a rotational analysis for many $^{130}Te_2$ transitions. This not only expands the reference frequency database, but also contributes to further investigations of tellurium and other homonuclear diatomic molecules. Here, transition lines from $B\ ({}^3\Sigma_u^-)\ 0_u^+ \leftarrow X\ ({}^3\Sigma_g^-)\ 0_g^+$ have been assigned via the $^{130}Te_2$ saturated absorption spectra in the range from 664154 to 676407 GHz. Dunham parameters and diatomic constants for the $B\ ({}^3\Sigma_u^-)\ 0_u^+$ state have been updated to an unprecedented level of precision. Our line assignment method for $^{130}Te_2$ can be adopted in other homonuclear

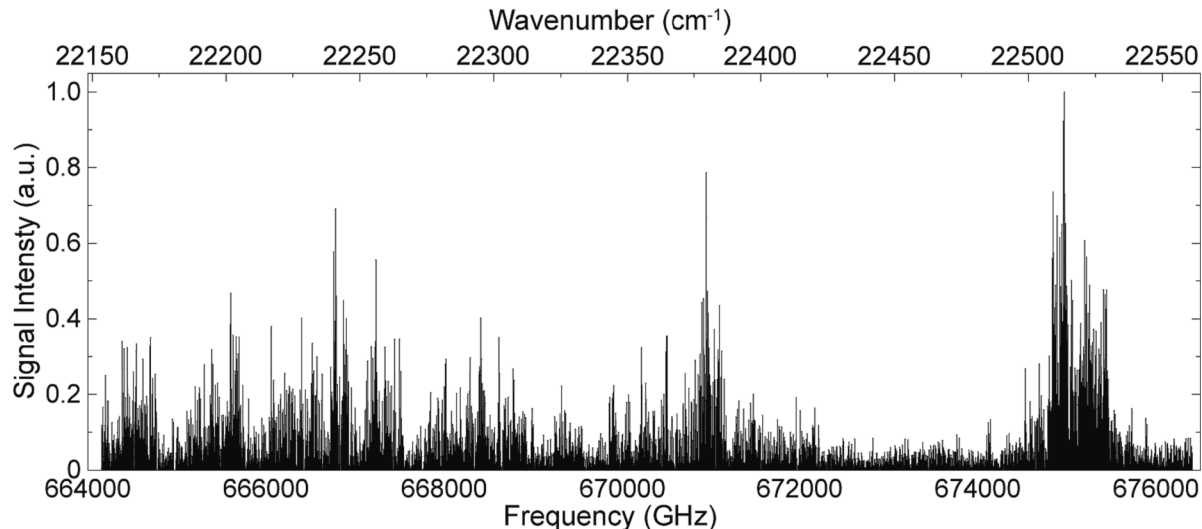


Fig. 3. Overall spectrum of $^{130}Te_2$ spanning the 443.2–451.4 nm region obtained via the Doppler-free SAS method.

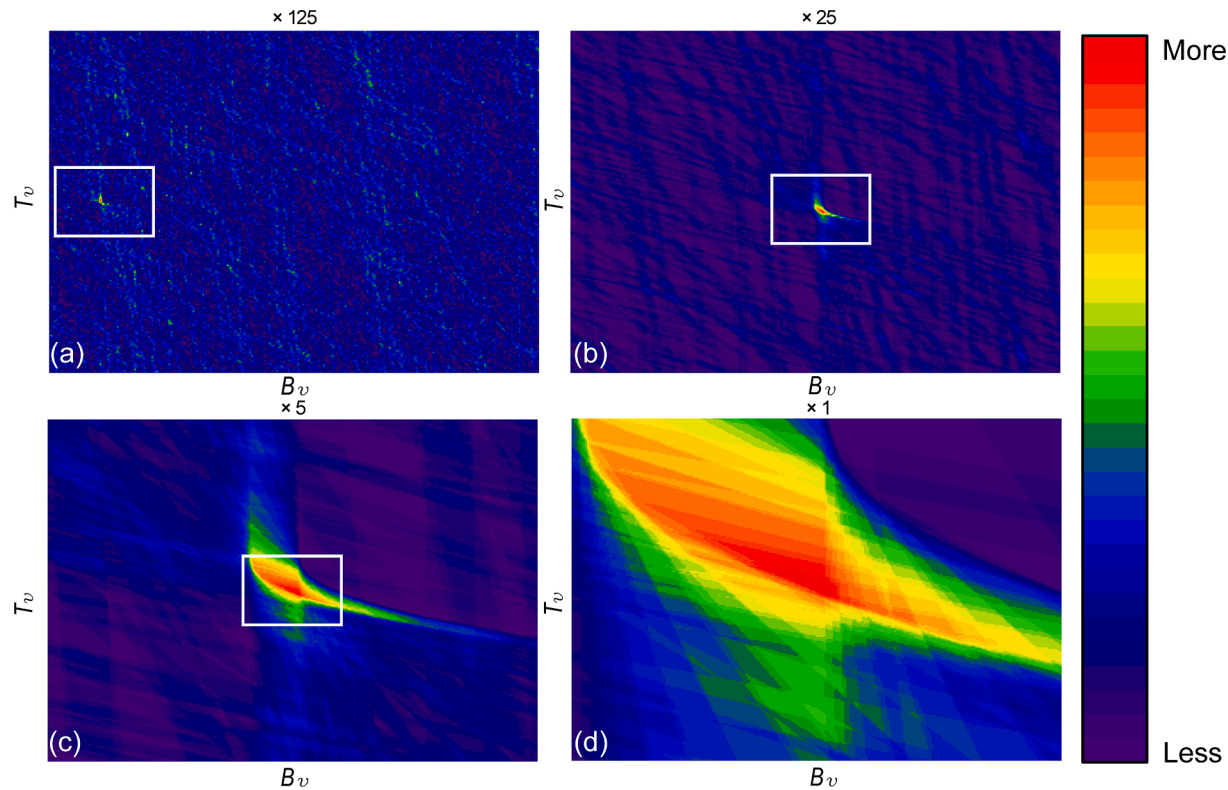


Fig. 4. Identification procedure for the $B\ ({}^3\Sigma_u^-)\ 0_u^+\ (v' = 4) \leftarrow X\ ({}^3\Sigma_g^-)\ 0_g^+\ (v = 1)$ transition lines. The four subpanels all manifest the grid size of 200×200 , however, the $[T_v, B_v]$ region are gradually zoomed in as the identification proceeds, which leads to four respective grid region of $(22927.66 \pm 0.5) \times (0.03197 \pm 0.00125)$, $(22927.265 \pm 0.1) \times (0.03197 \pm 0.00025)$, $(22927.269 \pm 0.02) \times (0.031965 \pm 0.00005)$, and $(22927.2698 \pm 0.004) \times (0.0319635 \pm 0.00001)$ in the units of $\text{cm}^{-1} \times \text{cm}^{-1}$. Each pixel represents a specific $[T_v, B_v]$ set and corresponds to a specific color indicating the number of matched lines found for this set of parameters. The white rectangle region outlines the scope of the next identification. (For interpretation of the references to color in this figure legend, the reader is referred to the web version of this article.)

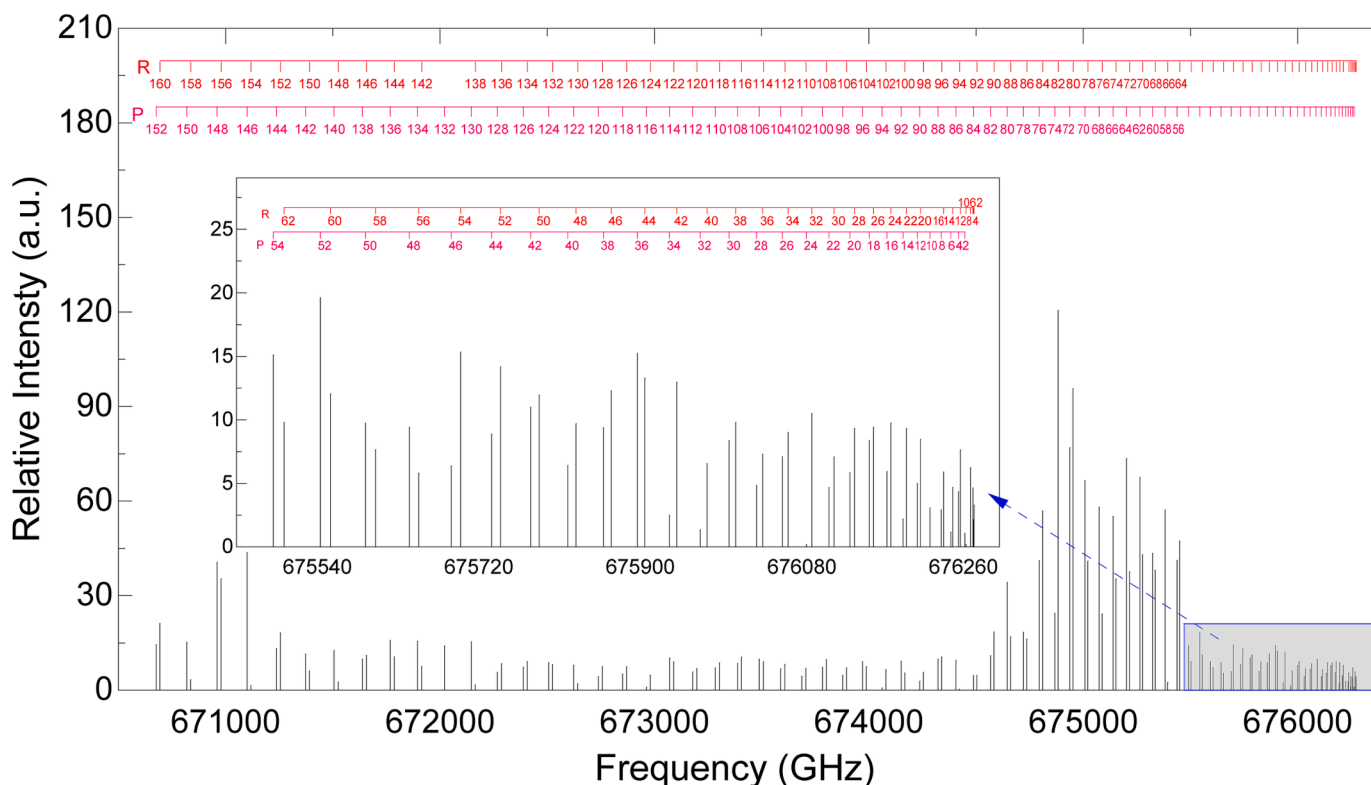


Fig. 5. Line assignment for the $B\ ({}^3\Sigma_u^-)\ 0_u^+\ (v' = 4) \leftarrow X\ ({}^3\Sigma_g^-)\ 0_g^+\ (v = 1)$ transition. The inset illustrates the assigned lines with low J values. Black: experimental results; Pink: assigned lines for the P branch; Red: assigned lines for the R branch. (For interpretation of the references to color in this figure legend, the reader is referred to the web version of this article.)

Table 1

Assignments for the $B\ (^3\Sigma_u^-)\ 0_u^+ (v' = 4) \leftarrow X\ (^3\Sigma_g^-)\ 0_g^+ (v = 1)$ transition of $^{130}\text{Te}_2$. The residuals between calculated and observed line frequencies Δ (Cal.-Obs.) are presented.

P branch ($\Delta J = -1$)						R branch ($\Delta J = +1$)					
J	Obs. (GHz)	Δ (MHz)	J	Obs. (GHz)	Δ (MHz)	J	Obs. (GHz)	Δ (MHz)	J	Obs. (GHz)	Δ (MHz)
2	676261.729	8.85	80	674644.985	4.71	2	676271.320	4.73	82	674882.594	-7.03
4	676254.727	9.28	82	674567.121	4.09	4	676271.986	5.53	84	674810.502	-8.66
6	676245.914	11.01	84	674487.422	6.75	6	676270.843	5.47	86	674736.570	-7.09
8	676235.295	8.20	86	674405.894	4.50	8	676267.891	4.23	88	674660.801	-6.82
10	676222.865	6.60	88	674322.529	5.31	10	676263.127	4.47	90	674583.198	-10.82
12	676208.625	5.10	90	674237.313	20.72	12	676256.555	2.64	92	674503.744	-5.46
14	676192.579	-0.79	92	674150.293	3.21	14	676248.165	7.55	94	674422.459	-11.20
16	676174.713	3.18	94	674061.411	10.30	16	676237.974	3.58	96	674339.311	2.91
18	676155.039	4.25	96	673970.696	9.45	20	676212.152	0.84	98	674254.273	62.14
20	676133.552	7.82	98	673878.134	14.40	22	676196.532	-8.91	100	674167.543	-33.04
22	676110.270	-4.92	100	673783.666	82.57	24	676179.082	-1.24	102	674078.861	-25.07
24	676085.160	-0.63	102	673687.516	-10.86	26	676159.830	-3.33	104	673988.337	-24.76
26	676058.248	-5.18	104	673589.419	-3.50	28	676138.762	-1.94	106	673895.962	-25.43
28	676029.520	-5.46	106	673489.478	-0.12	30	676115.892	-11.68	108	673801.732	-24.01
30	675998.974	-1.00	108	673387.691	0.82	32	676091.195	-8.36	110	673705.655	-30.30
32	675966.627	-7.16	110	673284.055	0.83	34	676064.693	-13.47	112	673607.712	-27.95
34	675932.457	-2.52	112	673178.565	1.16	36	676036.370	-13.27	114	673507.913	-28.67
36	675896.476	-1.09	114	673071.222	0.40	38	676006.235	-14.50	116	673406.255	-31.02
38	675858.686	-3.72	116	672962.021	2.11	40	675974.283	-15.88	118	673302.733	-32.24
40	675819.079	-3.86	118	672850.967	-1.64	42	675940.509	-10.40	120	673197.346	-33.63
42	675777.660	-6.22	120	672738.054	-6.84	44	675904.928	-14.65	122	673090.091	-33.76
44	675734.427	-10.32	122	672623.271	-3.53	46	675867.522	-11.28	124	672980.972	-39.08
46	675689.376	-11.51	124	672506.627	-4.04	48	675828.302	-12.33	126	672869.979	-42.51
48	675642.504	-7.78	126	672388.118	-4.97	50	675787.259	-9.30	128	672757.108	-42.47
50	675593.814	-3.34	128	672267.738	-4.60	52	675744.404	-12.72	130	672642.356	-37.07
52	675543.312	-4.64	130	672145.486	-2.88	54	675699.726	-14.13	132	672525.738	-46.12
54	675490.990	-4.15	132	672021.362	-2.30	56	675653.228	-16.50	134	672407.231	-47.33
56	675436.851	-5.56	134	671895.363	-3.80	58	675604.901	-11.50	136	672286.839	-48.54
58	675380.889	-3.22	136	671767.482	-1.45	60	675554.756	-11.30	138	672164.547	-37.89
60	675323.110	-4.50	138	671637.720	0.77	62	675502.792	-15.42	142	671914.335	-63.53
62	675263.507	-2.99	140	671506.070	5.95	64	675448.997	-12.95	144	671786.367	-58.44
64	675202.082	-1.71	142	671372.557	-12.75	66	675393.379	-12.05	146	671656.505	-60.54
66	675138.840	-6.12	144	671237.139	-17.91	68	675335.933	-10.47	148	671524.733	-58.17
68	675073.766	-2.32	146	671099.814	-9.86	70	675276.661	-10.63	150	671391.055	-57.25
70	675006.869	-0.23	148	670960.597	-6.70	72	675215.561	-10.36	152	671255.462	-55.32
72	674938.153	-4.81	150	670819.479	-4.33	74	675152.556	65.48	154	671117.955	-55.12
74	674867.600	1.76	152	670676.456	-1.40	76	675087.873	-11.24	156	670978.530	-60.06
76	674795.224	2.44				78	675021.279	-9.24	158	670837.171	-56.39
78	674721.019	3.39				80	674952.855	-9.90	160	670693.886	-59.46

diatomic molecules, and more importantly, from 443.2 to 451.4 nm can be utilized in other precision measurements, e.g. the non-zero *e*EDM measurement toward understanding parity and time-reversal symmetry violating effects in fundamental physics beyond the Standard Model [30].

2. Experimental setup

The experimental procedure has been described previously [18,29,31], while a brief synopsis of the experimental apparatus is presented here, including the stabilized frequency system and the Doppler-free SAS setup. The stabilized frequency system has been visualized in Fig. 1. The Toptica TA-SHG Pro laser provided the fundamental laser (~890 nm) whose IR output was split and sent to the wavemeter (Burleigh WA-1000) and the evacuated Fabry-Pérot (F-P) cavity (Toptica FPI-100), respectively. Sidebands were introduced upon the infrared (IR) beam to generate markers by connecting two electro-optical modulators (EOMs, a fiber coupled EOM at 200 MHz and a Thorlabs EO-PM-NR-C1 at 25 MHz) in series, which was then detected by a photodiode (PD, Thorlabs PDB210A). The frequencies for both EOMs were generated by frequency synthesizers utilizing the same 10 MHz GPS disciplined oscillator. The optical resonator used was actively held resonant to a Zeeman-stabilized HeNe laser (Micro-G LaCoste, ML-1) by means of a Pound-Drever-Hall (PDH) lock (Lock 1) [32]. The

transmission of the 200 MHz EOM was controlled via a standard servo lock (Lock 2) that adjusts the DC bias to enhance the relative sideband intensity. The cavity was thermally stabilized via the thermoelectric cooling (TEC) device to minimize the piezo voltage of the Fabry-Pérot cavity (Lock 3) using a thermistor. Finally, another PDH lock was used to lock the IR beam to the F-P cavity for precise frequency calibration, and for determining the free spectral range (FSR) of the F-P cavity. This lock was also used to measure frequency stability and accuracy by carefully measuring the D1 lines of Cs. Details of this investigation are included in the Supplemental Material [33].

The Doppler-free SAS setup surrounding the tellurium cell is illustrated in Fig. 2. The isotopically pure $^{130}\text{Te}_2$ was uniformly heated in a cylindrical glass cell maintained at 650 °C. With two laser beams prorogating in the same path but opposite directions through the cell, the spectrum was acquired via the SAS method. The “pump” and “probe” beams were created by dividing the original blue laser with a polarizing beam splitter (PBS). The pump laser passed through an EOM, $\lambda/2$ and $\lambda/4$ waveplate and another PBS to produce amplitude modulated light prior to entering the tellurium cell. The probe light was reflected by two mirrors and one PBS to pass through the cell. A photodiode was used to detect the SAS signal which was then demodulated by a lock-in amplifier.

Table 2

Numbers of assigned lines of P and R branches for the electronic transition $B(^3\Sigma_u^-) 0_u^+ \leftarrow X(^3\Sigma_g^-) 0_g^+$. The minimum and maximum numbers of assigned J 's for each branch are indicated as J_{MIN} and J_{MAX} individually, along with the identified numbers of transitions for P and R branches N_p and N_r . The number of total assigned lines is 1899, excluding those transitions labeled with the asterisk.

v	v'	P branch ($\Delta J = -1$)			R branch ($\Delta J = +1$)			$N_p + N_r$
		J_{MIN}	J_{MAX}	N_p	J_{MIN}	J_{MAX}	N_r	
1	3	8	82	35	14	82	33	68
1	4	2	188	93	2	196	95	188
2	4	2	80	40	2	88	44	84
2	5	2	160	77	0	168	82	159
2	6	86	126	20	94	130	17	37
3	5	2	92	45	0	100	51	96
3	6	2	118	55	0	126	61	116
3	7	2	140	69	0	148	74	143
4	7	8	68	27	14	74	30	57
4	9	64	148	39	72	156	37	76
5	8	2	76	36	0	84	42	78
5	9	6	106	49	2	116	56	105
5	10	4	78	37	2	78	38	75
6	11	8	72	32	4	70	33	65
6	12	2	156	78	2	160	80	158
7	11	4	44	21	0	52	26	47
7	12	4	82	38	2	90	43	81
8	13	6	50	21	8	52	20	41
8*	14*	10	30	6	—	—	—	6
8*	15*	8	36	8	8	34	5	13
9	16	12	128	50	10	130	55	105
9	17	4	130	62	2	126	58	120

3. Scanning results

This atlas contains 9294 lines ranging from 664154 to 676407 GHz (see Fig. 3). All the scanning results are then fitted with a Lorentzian line profile $y = \frac{A}{\pi} \frac{\gamma}{\gamma^2 + (x-x_0)^2}$, where A , 2γ and x_0 represent the relative amplitude, the full-width at half maximum (FWHM) of each transition line, and the central frequency, respectively. This atlas is archived in the [Supplemental Material](#).

In our experiment, the uncertainty for the frequency measurement originates from the detection reproducibility, the pressure shift from the gaseous $^{130}\text{Te}_2$ and the FSR evaluation. Uncertainty in the line position reproducibility is less than 1 MHz while the uncertainty in the vapor pressure shift [33] is ~ 1.8 MHz. The standard deviation of the absolute frequency relies on the measurement of the F-P cavity FSR and the distance between this line and the external frequency reference (Cesium D1 lines) [34]. The minimum is 200 kHz (from short-range standard deviation) while the maximum reaches 30 MHz at the extreme edges (664154–676407 GHz) within the ± 6 THz range. The pressure shift for $^{130}\text{Te}_2$ vapor at 650 °C is a systematic error estimated as -6 MHz [33]. The systematic pressure shift was applied to the data for the $^{130}\text{Te}_2$ spectroscopy and the fitted origins of the vibrational bands T_v . The overall uncertainty, including the short-range, long-range and absolute ones, is calculated to be 2 MHz at the center and 32 MHz at the extreme edges within the ± 6 THz range. A more detailed discussion of spectroscopic uncertainty, frequency calibration and errors is included in the [Supplemental Material](#).

4. Spectral line assignment

4.1. Line assignment procedure

The Dunham parameters and diatomic constants for the $X(^3\Sigma_g^-) 0_g^+$ and $B(^3\Sigma_u^-) 0_u^+$ states of $^{130}\text{Te}_2$ have been reported previously [14], where a variety of $B(^3\Sigma_u^-) 0_u^+ \leftarrow X(^3\Sigma_g^-) 0_g^+$ transitions were identified within our range. Because $^{130}\text{Te}_2$ has a center of inversion and $\Omega = 0$ for all states involved here, only P and R branches are allowed [29]. Before

we explain the procedure we present a brief explanation of the Dunham model [35] which was applied to the experimental transition lines for the energy level calculations. This Dunham model is used to describe the ro-vibrational energy level structure because $^{130}\text{Te}_2$ is a Hund's case c molecule and these transitions are combined rotation and vibration transitions. The model is characterized by its polynomial expansion parameters (Dunham parameters) as in Eq. (1), where T_v , B_v , D_v stand for the vibrational band origin, the rotational constant, and the centrifugal distortion constant respectively, with H_v , L_v and M_v standing for parameters of higher corrections. T_v and B_v can be derived from diatomic spectroscopic constants and represented as in Eqs. (2) and (3).

$$E_{v,J} = T_v + B_v J(J+1) - D_v (J(J+1))^2 + H_v (J(J+1))^3 + L_v (J(J+1))^4 + M_v (J(J+1))^5 \dots, \quad (1)$$

$$T_v = T_e + \omega_e \left(v + \frac{1}{2} \right) - \omega_e x_e \left(v + \frac{1}{2} \right)^2 + \omega_e y_e \left(v + \frac{1}{2} \right)^3 + \dots, \quad (2)$$

$$B_v = B_e - \alpha_e \left(v + \frac{1}{2} \right) + \dots. \quad (3)$$

Here, v and J stand for the vibrational and rotational quantum numbers, respectively. ω_e is the equilibrium vibrational frequency, $\omega_e x_e$ and $\omega_e y_e$ are corrections to ω_e that take into account the anharmonicity of the potential, B_e is the equilibrium rotational constant, and α_e is a constant determined by the shape of the anharmonic potential.

While 9294 lines were measured, only a portion of them were identified as $B(^3\Sigma_u^-) 0_u^+ \leftarrow X(^3\Sigma_g^-) 0_g^+$ transitions. An updated algorithm is elucidated here based on the method adopted in Ref. [17]. Previously reported Dunham parameters [12] were used as initial fitting parameters, and then optimized to obtain the maximum number of matched lines. The ground state parameters were treated as invariants, whereas the T_v and B_v in the $B(^3\Sigma_u^-) 0_u^+$ state varied within a certain range which is visualized as a grid. Transition lines with low J values (from 0 to 30) of the ground state are computed and compared for each $[T_v, B_v]$ set to determine if there is a match (at least one experimental transition line matched within the tolerance range). After finishing all the $[T_v, B_v]$ sets, the number of matched lines will be compared and the grid region of ideally fitted $[T_v, B_v]$ sets can be determined, which is then adopted as the searching scope of next fitting iteration. We repeated this method four times and generated a heat map as in Fig. 4, which illustrates the identification procedure for the $B(^3\Sigma_u^-) 0_u^+ (v' = 4) \leftarrow X(^3\Sigma_g^-) 0_g^+ (v = 1)$ transition lines. Such an identification method may also be utilized for the spectroscopic analysis of other diatomic molecules such as iodine.

After $[T_v, B_v]$ sets in the excited state have been optimized to fit most transition lines originating from lower J values in the ground state, iterative fitting was performed for higher J values. We first calculated Dunham parameters from matched lines (up to J_i) and used this set of parameters to predict transition lines for the next J value (J_{i+2}). During the process, the matched line list changed in every iteration. After each iteration a set of Linear Least Squares fits were performed to determine the optimized Dunham parameters and the number of parameters appropriate for the set of lines. Such iterations ceased when no matched lines could be found for the next consecutive J value.

Fig. 5 illustrates the overall assignment by labeling P (pink) or R (red) branch with respect to J , and Table 1 summarizes all assignment lines for the $B(^3\Sigma_u^-) 0_u^+ (v' = 4) \leftarrow X(^3\Sigma_g^-) 0_g^+ (v = 1)$ transition. Such an identification procedure was then used for searching other $B(^3\Sigma_u^-) 0_u^+ \leftarrow X(^3\Sigma_g^-) 0_g^+$ transitions, and the complete assignment can be found in the [Supplemental Material](#).

Table 3

Vibrational terms (T_v), rotational constants (B_v) and higher corrections of Dunham parameters for the B ($^3\Sigma_u^-$) 0_u^+ states of $^{130}\text{Te}_2$. The result has removed the effect of pressure shift for $^{130}\text{Te}_2$ vapor at 650 °C. Numbers in parentheses indicate twice the standard deviations in the last one or two digit(s).

v'	T_v (cm $^{-1}$)		
	This work	Vergès [14]	Barrow [12]
3	22768.68669(16)	-	-
4	22927.26661(24)	-	-
5	23084.477545(71)	23083.531(53)	23084.51
6	23240.29213(76)	-	23240.37
7	23394.68607(56)	23394.932(34)	23394.95
8	23547.547250(21)	23553.595(46)	23547.56
9	23699.04615(75)	23669.091(39)	23699.05
10	23848.93652(36)	-	23848.96
11	23997.23592(15)	-	23997.29
12	24143.89077(71)	-	24143.92
13	24288.76591(49)	-	24288.77
16	24712.601938(56)	24712.427(43)	24712.51
17	24849.83150(36)	-	24849.81

v'	$10^2 \times B_v$ (cm $^{-1}$)		
	This work	Vergès [14]	Barrow [12]
3	3.214290(51)	-	-
4	3.197583(18)	-	-
5	3.181409(71)	3.19459(47)	3.183
6	3.16118(14)	-	3.161
7	3.170190(72)	3.16176(16)	3.162
8	3.1463061(87)	3.14398(6)	3.146
9	3.12905(15)	3.12774(37)	3.13
10	3.10657(15)	-	3.108
11	3.107871(74)	-	3.105
12	3.087990(71)	-	3.088
13	3.07050(39)	-	3.074
16	3.02447543(83)	3.02435(11)	3.025
17	3.004946(59)	-	3.006

v'	Higher order corrections			
	$-10^9 \times D_v$ (cm $^{-1}$)	$10^{13} \times H_v$ (cm $^{-1}$)	$10^{17} \times L_v$ (cm $^{-1}$)	$10^{22} \times M_v$ (cm $^{-1}$)
3	7.13(48)	0.8(18)	-1.1 (30)	5.1(17)
4	6.422(34)	-0.130(24)	0.0346(74)	-0.1008(78)
5	6.76(18)	-0.65(18)	-0.220(72)	-0.97(10)
6	18.33(61)	10.6(11)	-20.66(77)	63.1(20)
7	17.92 (24)	7.22(29)	-2.49(15)	3.46(29)
8	7.603(91)	0.29(36)	-0.27(60)	1.7(36)
9	7.17(79)	-1.5(16)	-0.9(13)	-4.8(40)
10	23.4(17)	2.6(75)	63.0(137)	39.6(887)
11	12.18(10)	5.0(53)	-5.7(118)	48.1(941)
12	7.10(20)	-0.75(20)	0.433(87)	-1.21(13)
13	7.6(92)	-33.9(852)	-335.8(3378)	-9457(4763)
16	8.479(34)	0.307(54)	-0.126(37)	0.089(89)
17	8.35(25)	-0.10(41)	-0.003(286)	-0.51(70)

Table 4

Diatomical constants for the B ($^3\Sigma_u^-$) 0_u^+ state of $^{130}\text{Te}_2$. Numbers in parentheses indicate twice the standard deviations in the last one or two digit(s).

Term	This work (cm $^{-1}$)	Pazyuk [3] (cm $^{-1}$)	Stolyarov [4] (cm $^{-1}$)	Barrow [12] (cm $^{-1}$)
T_e	22204.71(66)	22202.83	22203.5(1.6)	22207.4
ω_e	163.11(23)	163.70	163.5(1.2)	162.32
$\omega_e x_e$	0.526(24)	0.587	0.563(45)	0.453
$\omega_e y_e$	-0.00899(76)	-0.00686	-0.042(9)	-0.01109
$10^2 \times B_e$	3.266(11)	3.255	3.258(40)	3.2535
$10^4 \times \alpha_e$	1.44(99)	1.28	1.35(5)	1.25

4.2. Identification and fitting results

Twenty ro-vibrational transition bands have been identified and numbers of assigned lines are tabulated in Table 2. Dunham parameters for the B ($^3\Sigma_u^-$) 0_u^+ ($v' = 3 - 17$) states of $^{130}\text{Te}_2$ have been calculated, and vibrational terms (T_v) as well as the associated rotational constants

(B_v) are compiled in Table 3. It is worth noting that when we applied more Dunham terms, spectroscopic lines involving B ($^3\Sigma_u^-$) 0_u^+ ($v' = 8$) exhibit better fitting outcome than those in previous studies [12,14,29]. The transitions involving v' of 14 and 15 could not be effectively assigned, indicating that corresponding Dunham parameters for the X ($^3\Sigma_g^-$) 0_g^+ ($v = 8$) state within our scan range may be inappropriately

chosen.

Based on optimized Dunham parameters and Eqs. (2) and (3), we are able to obtain diatomic constants for the $B(^3\Sigma_u^-)$ 0_u^+ state as summarized in Table 4.

5. Conclusion

To summarize, a Doppler-free SAS atlas which contains 9294 transition lines from 664154 to 676407 GHz for molecular $^{130}\text{Te}_2$ is presented, and 1899 $B(^3\Sigma_u^-)$ $0_u^+ \leftarrow X(^3\Sigma_g^-)$ 0_g^+ transition lines were identified using an iterative identification method. Optimized Dunham parameters of the $B(^3\Sigma_u^-)$ 0_u^+ state were obtained using the Linear Least Squares fitting, followed by updating the molecular constants of the $B(^3\Sigma_u^-)$ 0_u^+ state. The high resolution spectroscopic atlas of $^{130}\text{Te}_2$ can be extended beyond the investigated range, while the line assignment method might be applicable in other homonuclear diatomic molecules. Our work here also offers a versatile frequency reference for applications including precision spectroscopic measurements that explore fundamental physics beyond the Standard Model.

CRediT authorship contribution statement

Qinning Lin: Methodology, Software, Validation, Formal analysis, Investigation, Writing – original draft, Visualization. **Jie Ma:** Methodology, Software, Validation, Formal analysis, Investigation, Writing – original draft, Visualization. **James Coker:** Methodology, Formal analysis, Data curation, Investigation. **Renjun Pang:** Formal analysis. **Zesen Wang:** Formal analysis. **J.E. Furneaux:** Conceptualization, Validation, Formal analysis, Investigation, Data curation, Writing – review & editing, Supervision. **Jianping Yin:** Formal analysis, Validation. **Tao Yang:** Conceptualization, Methodology, Investigation, Resources, Writing – review & editing, Supervision, Project administration, Funding acquisition.

Declaration of Competing Interest

The authors declare that they have no known competing financial interests or personal relationships that could have appeared to influence the work reported in this paper.

Data availability

Data presented in this paper is archived in the ASCII file, named as "Atlas.txt".

Acknowledgements

We thank the support from the National Natural Science Foundation of China (12274140, 12034008, 12250003 and 91536218), the Shanghai Natural Science Foundation (22ZR1421400), the Fundamental Research Funds for the Central Universities, the Program for Professor of Special Appointment (Eastern Scholar) at Shanghai Institutions of Higher Learning, the Young Top-Notch Talent Support Program of Shanghai, and the Overseas Expertise Introduction Project for Discipline Innovation (the 111 Project, Code B12024).

Appendix A. Supplementary material

Supplementary material to this article, can be found online at <https://doi.org/10.1016/j.saa.2024.123887>.

References

- [1] M. Auzinsh, I. Klinicare, A. Stolyarov, Y. Tamanis, R. Ferber, Occurrence of circular polarization in Te_2 fluorescence due to quadratic Zeeman effect, in: High Resolution Molecular Spectroscopy: 11th Symposium and School, 1994, p. 2205.
- [2] E. Boursey, J. Meziane, A. Topouzhanian, Superfluorescence dynamics in $^{130}\text{Te}_2$, *IEEE J. Quantum Electron.* 29 (1993) 1038–1041.
- [3] E.A. Pazyuk, A.V. Stolyarov, M.Y. Tamanis, R.S. Ferber, Global deperturbation analysis from energetic, magnetic, and radiative measurements: application to Te_2 , *J. Chem. Phys.* 99 (1993) 7873–7887.
- [4] A.V. Stolyarov, E.A. Pazyuk, L.A. Kuznetsova, Y.A. Harya, R.S. Ferber, Effects of perturbations on the term values, Landé factors of $B 0_u^+$ and $A 1_u$ states and on intensities of $B 0_u^+ - X 1_g$ transitions of $^{130}\text{Te}_2$, *Chem. Phys. Lett.* 166 (1990) 290–294.
- [5] I. Klintsare, M. Tamanis, R. Ferber, Determination of lifetime and cross-section for relaxation of a Te_2 ($A 1_g$) molecule by the Hanle-effect method, *Optika i Spektroskopiâ* 67 (1989) 1222–1223.
- [6] I. Klintsare, A. Stolyarov, M.Y. Tamanis, R. Ferber, Y.A. Khar'ya, Anomalous behaviour of Te_2 ($B 0_u^+$)-molecule Landé factors and $B 0_u^+ - X 1_g$ transition intensities, *Optika i Spektroskopiâ* 66 (1989) 1018–1021.
- [7] R. Viswanathan, M.S. Baba, D.D. Albert Raj, R. Balasubramanian, T.S. L. Narasimhan, C.K. Mathews, A mass spectrometric study of the dissociation of the gaseous diatomic tellurium molecule, *Spectrochim. Acta Part B* 49 (1994) 243–250.
- [8] A. Arie, S. Schiller, E.K. Gustafson, R.L. Byer, Absolute frequency stabilization of diode-laser-pumped Nd: YAG lasers to hyperfine transitions in molecular iodine, *Opt. Lett.* 17 (1992) 1204–1206.
- [9] Y. Makdisi, K.S. Bhatia, Ultraviolet and visible spectra of tellurium I, *J. Phys. B* 15 (1982) 909–913.
- [10] J.D. Gillaspy, J. Feinberg, B. Fischer, C.J. Sansonetti, Absolute wavelength determinations in molecular tellurium: new reference lines for precision laser spectroscopy: errata, *J. Opt. Soc. Am. B* 9 (1992) 2414–2419.
- [11] J. Cariou, P. Luc, *Atlas du Spectre d'Absorption de la Molécule Tellure*, Partie 5: 21,100–23,800 cm^{-1} in, CNRS, 1980, pp. 70.
- [12] R. Barrow, R. Du Parcq, Rotational analysis of the $A 0_u^+$, $B 0_u^+$ - $X 0_g^+$ systems of gaseous Te_2 , *Proc. R. Soc. Lond. A* 327 (1972) 279–287.
- [13] K.K. Yee, R.F. Barrow, Observations on the absorption and fluorescence spectra of gaseous Te_2 , *J. Chem. Soc. Faraday Trans. 2* (68) (1972) 1397–1403.
- [14] J. Vergès, C. Effantin, O. Babaky, J. d'Incan, S.J. Prosser, R.F. Barrow, The laser induced fluorescence spectrum of Te_2 studied by fourier transform spectrometry, *Phys. Scr.* 25 (1982) 338–350.
- [15] J. Vergès, J. d'Incan, C. Effantin, D.J. Greenwood, R.F. Barrow, Laser-excited fluorescence of gaseous Te_2 studied by Fourier transform spectrometry, *J. Phys. B* 12 (1979) L301–L304.
- [16] E. Martínez, F.J. Basterrechea, P. Puyuelo, F. Castano, Fluorescence decay lifetimes of the $B(0_u^+)$ and $A(0_u^+)$ states of Te_2 , *J. Phys. B* 23 (1990) 77–84.
- [17] Q. Lin, R. Pang, Z. Wang, S. Hou, H. Wang, J. Yin, T. Yang, High resolution spectroscopic measurement of $^{130}\text{Te}_2$: Reference lines near 444.4 nm for eEDM experiment using PbF molecules, *Spectrochim. Acta A: Mol. Biomol. Spectrosc.* 270 (2022) 120754.
- [18] J. Coker, H.Q. Fan, C.P. McRaven, P.M. Rupasinghe, T.Z. Yang, N.E. Shafer-Ray, J. E. Furneaux, Cavity dispersion tuning spectroscopy of tellurium near 444.4 nm, *J. Opt. Soc. Am. B* 28 (2011) 2934–2939.
- [19] T. Dutta, D. De Munshi, M. Mukherjee, Absolute Te_2 reference for barium ion at 455.4 nm, *J. Opt. Soc. Am. B* 33 (2016) 1177–1181.
- [20] T. Dutta, M. Mukherjee, High resolution spectroscopy on Te_2 : New lines for reference, *Spectrochim. Acta Part A* 208 (2019) 109–113.
- [21] I.S. Burns, J. Hult, C.F. Kaminski, Use of $^{130}\text{Te}_2$ for frequency referencing and active stabilisation of a violet extended cavity diode laser, *Spectrochim. Acta Part A* 63 (2005) 905–909.
- [22] U. Dammalapati, K.-I. Harada, T. Inoue, S. Ito, H. Kawamura, K. Sakamoto, K. Tanaka, A. Uchiyama, R. Yoshioka, Y. Sakemi, Frequency measurement of tellurium lines near calcium, *J. Phys. Soc. Jpn.* 86 (2017) 124301.
- [23] D.H. McIntyre, T.W. Hänsch, Interferometric frequency measurement of a $^{130}\text{Te}_2$ reference line for muonium 1S–2S spectroscopy, *Phys. Rev. A* 36 (1987) 4115–4118.
- [24] D.H. McIntyre, T.W. Hänsch, Absolute calibration of the $^{130}\text{Te}_2$ reference line for positronium 1^3S_1 - 2^3S_1 spectroscopy, *Phys. Rev. A* 34 (1986) 4504–4507.
- [25] T.J. Scholl, S.J. Rehse, R.A. Holt, S.D. Rosner, Absolute wave-number measurements in $^{130}\text{Te}_2$: Reference lines spanning the 420.9–464.6 nm region, *J. Opt. Soc. Am. B* 22 (2005) 1128–1133.
- [26] P. Cancio, D. Bermejo, Absolute wavelengths in $^{130}\text{Te}_2$: New reference lines for laser spectroscopy coinciding with emissions of the Ar^+ laser, *J. Opt. Soc. Am. B* 14 (1997) 1305–1311.
- [27] L.S. Ma, P. Courteille, G. Ritter, W. Neuhauser, R. Blatt, Spectroscopy of Te_2 with modulation transfer: reference lines for precision spectroscopy in Yb^+ at 467 nm, *Appl. Phys. B* 57 (1993) 159–162.
- [28] J.R.M. Barr, J.M. Girkin, A.I. Ferguson, G.P. Barwood, P. Gill, W.R.C. Rowley, R. C. Thompson, Interferometric frequency measurements of $^{130}\text{Te}_2$ transitions at 486 nm, *Opt. Commun.* 54 (1985) 217–221.
- [29] D.L. Mantia, A Highly Stable and Repeatable Source for Spectroscopy of the $B 0_u^+$ - $X 0_g^+$ Transitions in $^{130}\text{Te}_2$, The University of Oklahoma, 2014, p. 103.
- [30] R.J. Mawhorter, B.S. Murphy, A.L. Baum, T.J. Sears, T. Yang, P.M. Rupasinghe, C. P. McRaven, N.E. Shafer-Ray, L.D. Alphei, J.-U. Grabow, Characterization of the ground X_1 state of $^{204}\text{Pb}^{19}\text{F}$, $^{206}\text{Pb}^{19}\text{F}$, $^{207}\text{Pb}^{19}\text{F}$, and $^{208}\text{Pb}^{19}\text{F}$, *Phys. Rev. A* 84 (2011) 022508.
- [31] J. Coker, Applications of Diatomic Molecules, The University of Oklahoma, Oklahoma, 2015.
- [32] E.D. Black, An introduction to Pound–Drever–Hall laser frequency stabilization, *Am. J. Phys.* 69 (2001) 79–87.

- [33] G.P. Barwood, W.R.C. Rowley, P. Gill, J.L. Flowers, B.W. Petley, Interferometric measurements of $^{130}\text{Te}_2$ reference frequencies for 1S–2S transitions in hydrogenlike atoms, Phys. Rev. A 43 (1991) 4783–4790.
- [34] T. Udem, J. Reichert, R. Holzwarth, T. Hänsch, Absolute optical frequency measurement of the cesium D1 line with a mode-locked laser, Phys. Rev. Lett. 82 (1999) 3568.
- [35] J.L. Dunham, The energy levels of a rotating vibrator, Phys. Rev. 41 (1932) 721–731.